

## Chloride penetration resistance of engineered cementitious composite (ECC) subjected to sustained flexural loading

Wang, Chuan; Sun, Renjuan; Hu, Xinlei; Guan, Yanhua; Yang, Yingzi; Lu, Wei; Tian, Jun; Zhang, Hongzhi; Ge, Zhi; Šavija, Branko

**DOI**

[10.1016/j.mtcomm.2023.106080](https://doi.org/10.1016/j.mtcomm.2023.106080)

**Publication date**

2023

**Document Version**

Final published version

**Published in**

Materials Today Communications

**Citation (APA)**

Wang, C., Sun, R., Hu, X., Guan, Y., Yang, Y., Lu, W., Tian, J., Zhang, H., Ge, Z., & Šavija, B. (2023). Chloride penetration resistance of engineered cementitious composite (ECC) subjected to sustained flexural loading. *Materials Today Communications*, 35, Article 106080. <https://doi.org/10.1016/j.mtcomm.2023.106080>

**Important note**

To cite this publication, please use the final published version (if applicable). Please check the document version above.

**Copyright**

Other than for strictly personal use, it is not permitted to download, forward or distribute the text or part of it, without the consent of the author(s) and/or copyright holder(s), unless the work is under an open content license such as Creative Commons.

**Takedown policy**

Please contact us and provide details if you believe this document breaches copyrights. We will remove access to the work immediately and investigate your claim.

***Green Open Access added to TU Delft Institutional Repository***

***'You share, we take care!' - Taverne project***

**<https://www.openaccess.nl/en/you-share-we-take-care>**

Otherwise as indicated in the copyright section: the publisher is the copyright holder of this work and the author uses the Dutch legislation to make this work public.



# Chloride penetration resistance of engineered cementitious composite (ECC) subjected to sustained flexural loading

Chuan Wang<sup>a</sup>, Renjuan Sun<sup>b,\*</sup>, Xinlei Hu<sup>c</sup>, Yanhua Guan<sup>b</sup>, Yingzi Yang<sup>d</sup>, Wei Lu<sup>b</sup>, Jun Tian<sup>a</sup>, Hongzhi Zhang<sup>b,e,\*\*</sup>, Zhi Ge<sup>b</sup>, Branko Šavija<sup>f</sup>

<sup>a</sup> Shandong Hi-speed Group Co. Ltd., 250014 Jinan, China

<sup>b</sup> School of Qilu Transportation, Shandong University, 250002 Jinan, China

<sup>c</sup> Chongqing Luneng Development Group Co, Ltd, 401336 Chongqing, China

<sup>d</sup> School of Civil Engineering, Harbin Institute of Technology, Harbin 150090, China

<sup>e</sup> Suzhou Research Institute, Shandong University, 215021 Suzhou, China

<sup>f</sup> Faculty of Civil Engineering and Geosciences, Delft University of Technology, 2628 CN Delft, the Netherlands

## ARTICLE INFO

### Keywords:

Engineered cementitious composites  
Chloride penetration behavior  
Sustained flexural load  
Maximum normal tensile stress  
Microcracks

## ABSTRACT

This paper presents a research on the chloride penetration behavior of engineered cementitious composites (ECC) under sustained flexural loads. Three load levels, i.e. 30 %, 60 % and 75 % of the ultimate flexural load were used. Chloride diffusion depth and concentration profile were measured 30, 60 and 150 days after the specimen was exposed to NaCl solution and compared with pre-loaded specimens. Influence of the sustained local bending stress and microcracks were investigated. It shows that under sustained loads, the relationship between the surface chloride content and maximum normal tensile stress can be described using an exponential equation. A binary model was developed to explain the correlation among the chloride ion diffusion coefficient, maximum normal tensile stress and exposure time. Changes of capillary pore structure and phase compositions were measured using mercury intrusion porosimeter and X-ray diffraction, respectively. Unlike mortar, the fiber bridging of ECC helps with limiting crack width and thus the diffusion process, and the measured results were used to explain the observed penetration behavior of ECC. It is believed that the current study provides theoretical foundation for the durable design of the ECC/concrete composite structure.

## 1. Introduction

The corrosion of reinforcement by chloride ions has been causing serious damage of reinforced concrete structures. The chloride exposure environment is not limited to marine environment where chloride concentration is in general close to 19 g/L. Near salty lakes, the chloride concentration can reach as high as 220 g/L [1]. A large number of efforts have been made to explain the mechanism of chloride transport [2–4]. Furthermore, it has been shown that cracks play an important part in chloride ingress. Raharinaivo et al. [5] exhibited that the diffusion rate of cracked concrete is tens to hundreds of times that of intact concrete. It is reported that showed that chloride ingress is significantly affected by cracks wider than 500  $\mu\text{m}$ , while crack less than 200  $\mu\text{m}$  width had nearly no effect [6]. Djerbi et al. [7] studied the effect of traversing crack on chloride ingress into concrete. The cracks between 30 and 250  $\mu\text{m}$

were created was created using splitting tensile tests. They concluded that the diffusion coefficient is proportional to the crack width. And the diffusion coefficient through the crack equals to that in the free solution, as the crack width exceeds 80  $\mu\text{m}$ .

Consequently, reducing crack width is considered as a positive way to improve the durability of reinforced concrete. Incorporation of an engineered cementitious composite (ECC) at the tensile side of the concrete member provides one promising solution [8–11] as ECC has excellent tensile ductility and limited crack width (less than 60  $\mu\text{m}$  when the strain is below 1 %) [12–14]. Through micromechanics-based material design, the ultimate tensile strain of ECC averagely exceed 3 %. This is 200–500 times of the normal concrete [15]. Leung et al. [16] revealed that the layered ECC/concrete beam shows great improvement in both static strength and fatigue performance. Izuka et al. [17] replaced part of the concrete at the tensile side of the unidirectional slab

\* Corresponding author.

\*\* Corresponding author at: School of Qilu Transportation, Shandong University, 250002 Jinan, China.

E-mail addresses: [sunrenjuan@sdu.edu.cn](mailto:sunrenjuan@sdu.edu.cn) (R. Sun), [hzzhang@sdu.edu.cn](mailto:hzzhang@sdu.edu.cn) (H. Zhang).

by ECC. As expected, crack width and spacing were remarkably decreased. In bridge engineering, ECC can be used directly on the deck paving of steel girder bridges. A steel-ECC composite deck structure can obviously increase the strength and stiffness of the slab with limited crack width [18–20].

In order to serve the durability design of such composite members accurately, an understanding of the chloride penetration behavior in ECC is required. The transport performance of ECC under chloride condition have been extensively studied in the past. Numerous studies have shown that because of the heavy use of fly ash and low water-to-cement ratio, the chloride ion diffusion coefficient of this material is smaller than that of concrete [21]. Furthermore, the impact of the stress level on the chloride diffusion behavior was studied [22–24], in which flexural and tensile forces were used to load the specimen. And the chloride diffusion coefficient was measured after unloading. It has been observed that self-healing occurs which results in a decrease in crack width during chloride exposure [25–27]. This leads to an improved chloride penetration resistance. However, in field conditions, the material is under sustained load, which causes further change of the microstructure [28,29]. Therefore, the influence of sustained load cannot be considered if the specimens are unloaded before chloride exposure. Kobayashi et al. [30] studied the corrosion of reinforcement inside the ECC with the pre-loaded and specimens subjected to sustained loading. As expected, different corrosion behaviors were observed. Therefore, to reveal the mechanism behind and provide fundamental data for the durability design of ECC-composite members, it is essential to investigate chloride transport behavior in ECC under sustained loading.

To this end, the current research studied the chloride diffusion performance of ECC under sustained flexural load. Three load levels, e.g. 30 % 60 % and 75 % of the ultimate flexural load were applied on prismatic ECC specimens. Chloride diffusion depth and content profile were measured when the specimens were immersed to NaCl solution for 30, 60 and 150 days. In the course of this experiment, the influence of the maximum normal tensile stress and microcracks was also investigated. And, changes of capillary pore structure and chemical compositions after the NaCl immersion were characterized using mercury intrusion porosimeter (MIP) and X-ray diffraction (XRD) respectively.

## 2. Materials and methods

### 2.1. Materials and specimens

The experimental materials include ordinary Portland 42.5 cement, Grade I fly ash, local quartz sand, and particle sizes of 125–180  $\mu\text{m}$ , polyvinyl-alcohol (PVA) fiber, Hypromellose-type viscosity modifying admixture (VMA) and polycarboxylic superplasticizer. The chemical component of the cement and FA used is measured by X-ray fluorescence (XRF), as shown in Table 1. The PVA fiber is from Kuraray company of Japan. The length, width and density of the fibers are respectively 12 mm, 40  $\mu\text{m}$  and 1.3  $\text{g}/\text{cm}^3$ . The mix proportion for ECC is summarized in Table 2. The dry ingredients and VMA were first added to the mixer and stirred slowly for 2 min. Then the water and water reducer were mixed well, added to the mixing pot and stirred quickly for 4 min. Finally, the fibers were added to the mixture and stirred slowly for another 4 min. Cuboid specimens in sizes of 400 mm  $\times$  100 mm  $\times$  60 mm were produced. Then they were cured in lime saturated water for 28 days.

**Table 1**

Chemical compositions of the cement and the fly ash (wt%) measured by XRF.

Oxide	CaO	SiO <sub>2</sub>	Al <sub>2</sub> O <sub>3</sub>	Fe <sub>2</sub> O <sub>3</sub>	MgO	SO <sub>3</sub>	Na <sub>2</sub> O	K <sub>2</sub> O	TiO <sub>2</sub>	MnO	P <sub>2</sub> O <sub>5</sub>
Cement	63.21	18.48	6.74	3.45	3.24	3.16	0.17	0.53	0.35	0.27	0.16
Fly ash	3.43	49.66	35.97	5.77	0.63	1.12	0.62	0.93	0.99	0.04	0.28

### 2.2. Determination of bending tensile strength

The flexural load bearing capacity was determined by the four-point flexural test. The length between the two supports was 300 mm. The experiment was conducted using a universal testing machine. The measuring range of the machine is 50 kN. In the test of bending tensile strength, a displacement control mode of 0.5 mm/min was adopted. During the test, the midspan deflection change of the specimen was measured by the linear variable differential transformer. The average ultimate bending load results from 4 specimens were applied as the flexural load capacity.

### 2.3. Loading conditions

Multiple stress levels (namely 30 %, 60 % and 75 % of the maximal flexural load) were applied in this study. Two loading conditions were considered for the exposure test. The first is termed as pre-loaded conditions, in which the specimens were subjected to flexural load prior to immersed in the NaCl solution. In the test, the specimens were loaded to the targeted stress value. Then, the flexural load was maintained for 15 min. Afterwards, the specimens were unloaded and subjected to the condition. The second considers the sustained loading conditions. The machine used to apply the load is shown in Fig. 1. This instrument can load 3 specimens at the same time [31]. The load was adjusted by controlling the nuts. At the same time, the applied pressure value was recorded by the sensor in real time. After the target load value was observed, it is necessary to adjust the bolt every day to guarantee the load value is unchanged. In order to reduce the impact of sample weight from the top on the bottom sample, the apparatus was laid horizontally in a container with NaCl solution.

### 2.4. Exposure conditions

The bottom of the prismatic specimen was used for loading and the other surfaces were sealed with epoxy resin. In this way, the chloride ion penetration can occur only from this side. After the solidification of the epoxy resin, the specimens were exposed in 10 % NaCl solution under a temperature of  $20 \pm 2$  °C. The specimens were taken out after 30, 60 and 150 days of immersion. This was followed by washing the residual NaCl solution from the specimen surface. The two loading conditions, three loading levels, three immersion durations together with the reference samples (without loading) results in a total of 21 testing conditions. For each condition, 3 specimens were measured. In total, 63 specimens were prepared and tested.

### 2.5. Sample collections

Under four-point bending loading condition, the flexural stress within the specimens varied with the distance to the supports. As depicted in Fig. 2, theoretically, the region between the two loading positions (i.e. C<sup>1</sup> and C<sup>2</sup>) was subjected to pure bending, where the bending moment was the highest along the span. In contrast, bending moments at position A and B are 0 % and 50 % of the maximum, respectively. To elucidate the effect of bending forces on chloride transport behavior in ECC, half of the specimens were cut at cross-sections A–B (i.e., area: 100 mm  $\times$  60 mm), where the penetration depth and content of chloride ions were measured. The other half of the specimen was cut through the X–X plane along span (i.e. area: 200 mm  $\times$  60 mm) as indicated in Fig. 2(c) to visualize the effect of the

**Table 2**  
Mix proportion of ECC.

Water-binder ratio	Water (kg/m <sup>3</sup> )	Cement (kg/m <sup>3</sup> )	Fly ash (kg/m <sup>3</sup> )	Quartz sand (kg/m <sup>3</sup> )	Fiber (kg/m <sup>3</sup> )	VMA (kg/m <sup>3</sup> )	Superplasticizer (kg/m <sup>3</sup> )
0.26	326	570	684	456	26.1	0.57	5.02

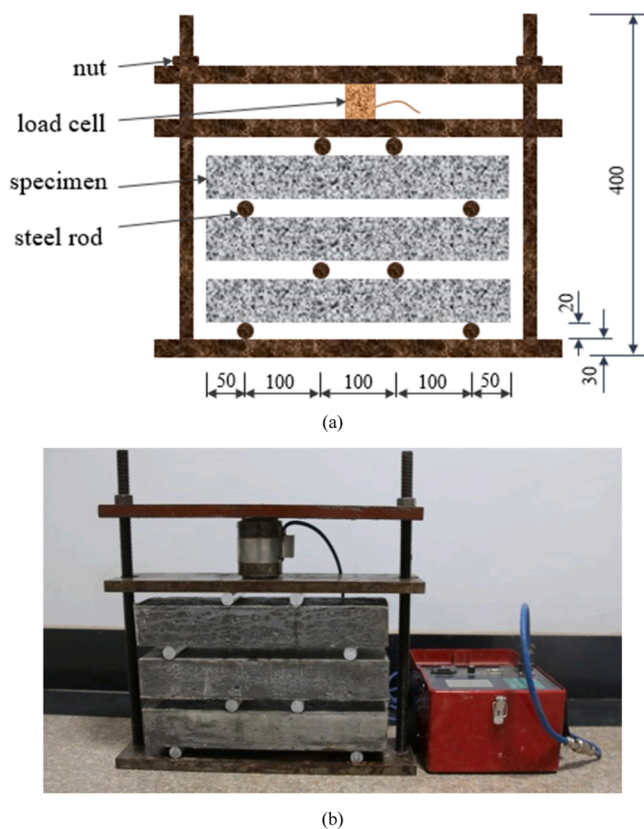


**Fig. 1.** Overview of the apparatus for the sustained loading (unit: mm): (a) schematic view; (b) specimens loaded by the apparatus.

cracking on the chloride penetration behavior.

## 2.6. Chloride penetration depth measurement

The chloride penetration depth was measured by the silver nitrate titration experiment. In the test, 0.1 mol/L of silver nitrate solution is applied to the cutting surface of the specimen, which resulted in the following two chemical reactions. On the one hand, silver chloride (AgCl) was formed at the area containing free chlorides (at 0.15 % above the mass ratio of cement [32]) resulting in white precipitation. On the other hand, brown silver oxide (Ag<sub>2</sub>O) precipitated [33–35]. The average depth of the white area can be regarded as the chloride penetration depth. In the current study, the white silver chloride position is divided by 9 aliquots. Then the values of 10 erosion depths are measured.

## 2.7. Chloride content measurement

In terms of the chloride content test, powders were collected using a vertical spindle drilling machine from the surface under tension with an interval of 5 mm. The chosen depths are 0–5 mm, 5–10 mm, 10–15 mm and 15–20 mm, respectively. The powder of each depth was sifted with a 0.15 mm sieve. The remaining powder was dried at 105 °C for 24 h. Afterwards, 2 g of powder was poured into 200 ml of distilled water. Then a magnetic stirrer was used to stir the solution for 10 min to allow the powder to fully dissolve. Finally, the NELD-CL420 chloride ion test

instrument was used to conduct the experiment.

## 2.8. XRD and MIP tests

For the X-ray diffraction (XRD) tests, two specimens were investigated for comparison. The first was the specimen exposed to water for 60 days with no load. The second was the specimen experienced 60 days coupled sustained load (75 % of the ultimate strength) and NaCl solution exposure. Powders were taken from the pure bending region within 5 mm depth of the surface under maximum tensile stress. To prevent further hydration, the samples were initially exposed in anhydrous ethanol for one day, followed by immersing for another 6 days in renewed anhydrous ethanol. After that, the samples were vacuum dried under 45 °C for 24 h, and then ground and sieved through a 0.075 mm sieve. Finally, the powders were vacuum dried under 45 °C for another 48 h. Mineral phases were investigated by X'Pert PRO X-ray diffractometer (Bruker, Germany) with Cu- K $\alpha$  radiation at 40 kV, 30 mA over a range from 5° to 55°. And the scanning speed is 0.017°/s.

Regarding the mercury intrusion porosimeter (MIP) tests, two specimens were tested. They were: 1) 28 days cured specimens with no loading; 2) 28 days cured specimen experienced 60 days' coupled sustained loading (75 % of the ultimate strength) and NaCl solution exposure. Before the test, the sample was exposed in anhydrous ethanol. Afterwards, the samples were placed in vacuum drying chamber under 45 °C for 48 h. The MIP tests were performed with Autopore II 9220 mercury intrusion porosimeter. The pressure range of the instrument is  $4.00 \times 10^{-3}$ – $4.13 \times 10^2$  MPa, corresponding to a pore size ranging from 7 nm to 314  $\mu$ m. The contact angle used in the MIP tests was taken as 130°.

## 3. Experimental results and discussion

### 3.1. Flexural capacity

The relationship between flexural load and midspan deflection under the four-point bending tests are exhibited in Fig. 3. Typical deflection-hardening behavior was observed. The early crack load and the ultimate flexural load are summarized in Table 3, and their average values were 8.89 kN and 13.70 kN, respectively, which is produced by four specimens. Therefore, the 13.70 kN is the base value for determining the load level.

### 3.2. Influence of load levels on chloride penetration

The measured chloride penetration depths at the pure bending zone (position C, see Fig. 2) are presented Fig. 4. Overall, it shows that the chloride penetration depth increased with the load level and the exposure time, as expected. The chloride penetration depth increment rate decreases with exposure time. The penetration depth was more considerable for specimens under the sustained loading condition than those pre-loaded specimens, and this difference increases over time. Specifically, for specimens exposed for 30 days, the chloride penetration depth of the sustained loaded specimens was only 6.3 %, 1.3 % and 2 % higher than the loaded and pre-loaded specimens under 30 %, 60 %, and 75 % of ultimate load level respectively. When the exposure time was 150 days, the differences increase up to 21.5 %, 21.6 %, and 17.8 %. This may be attributed to the different autogenous self-healing capacity which results in smaller cracks or even closed cracks [25–27]. It is expected autogenous self-healing become less pronounced in specimens under continuous loading because the cracks are wider.

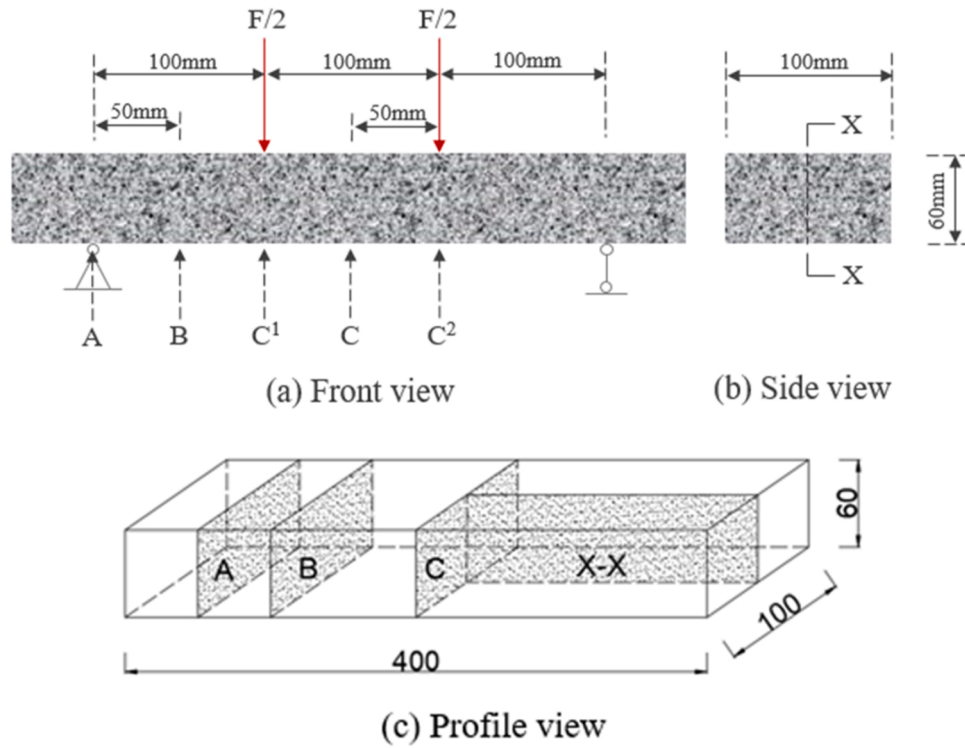


Fig. 2. Schematic view for the sample collections.

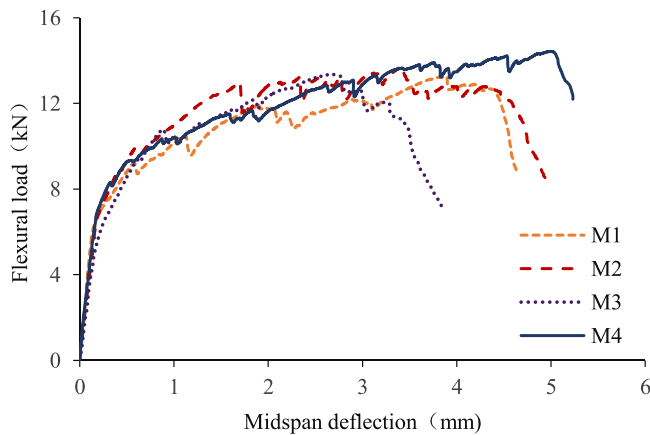


Fig. 3. Flexural load-midspan deflection curves.

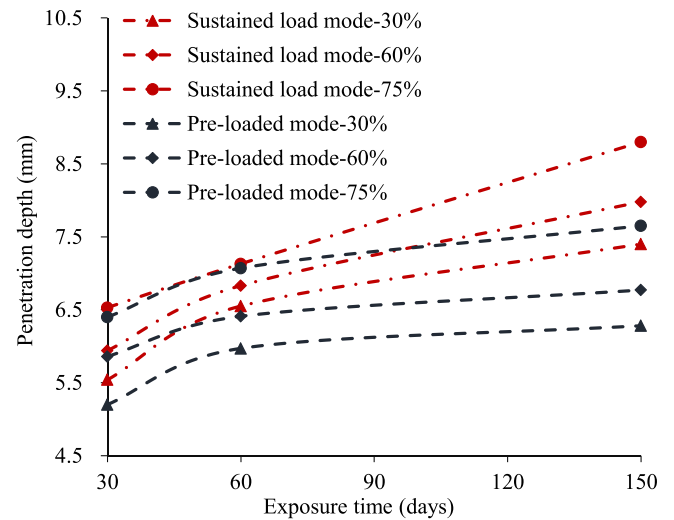


Fig. 4. Evolution of the chloride penetration depths over exposure time at C profile.

**Table 3**  
Flexural strength of ECC specimens (28 days).

Name	First-cracking load (kN)	Ultimate load (kN)	First-cracking strength (MPa)	Ultimate strength (MPa)
M1	9.24	13.27	7.70	11.06
M2	8.60	13.72	7.17	11.43
M3	9.40	13.36	7.83	11.13
M4	8.32	14.43	6.93	12.03
Average	8.89	13.70	7.41	11.41
Standard deviation	0.44	0.46	0.37	0.38

In addition, more significant increment of the chloride penetration depth was found when the load level raised from 60 % to 75 % compared with the load levels between 30 % and 60 %. This is due to the fact that, at the load levels between 30 % and 60 % of the ultimate

flexural load, the material almost stays in the elastic stage and only a few cracks are present. When the load increases from 60 % to 75 % of the ultimate flexural load, ECC is in the deflection hardening stage in which multiple microcracks form. The microcracks provide accessible channels for the transport of chloride ions in the ECC matrix, thus accelerating the chloride ingress [36].

The influence of the sustained load level on chloride ion concentration (at C profile) after 60 days of immersion is shown in Fig. 5. Clearly, with the increase of load level, the chloride concentration increased at each test depth. The surface chloride concentrations measured at 30 %, 60 % and 75 % of ultimate load are 0.84 %, 1.02 % and 1.34 %, respectively. Under 30 % and 60 % of the ultimate load, the chloride content at the 10–20 mm depth was similar. However, a considerable

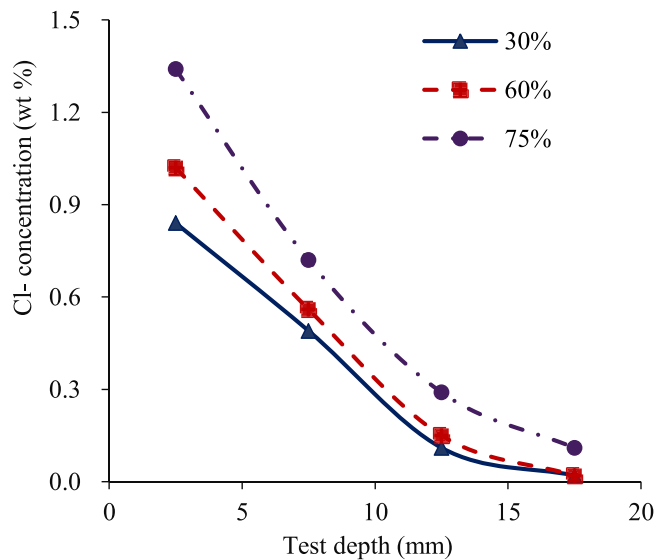


Fig. 5. Influence of the sustained load level on chloride profile (at pure bending region) after immersion of 60 days at C area.

increment was found for specimens under 75 % of the ultimate loading. This can be explained by the formation of the multiple cracks at 75 % of the ultimate load level, which creates more channels for the intrusion of chloride ions.

Fig. 6 compares the chloride concentration profile under different loading modes at 60 days in the pure bending region. The chloride concentration within 10 mm depth was significantly different between the two loading conditions. In terms of the pre-loaded condition, they were 0.37 %, 0.47 % and 0.55 % for 30 %, 60 % and 75 % of the ultimate load, respectively. The chloride concentrations rose up to 0.67 %, 0.79 % and 1.03 % for the sustained load condition, which were 1.78, 1.67 and 1.88 times of the pre-loaded mode. This difference gradually decreased with the depth increasing, especially for the load level of 30 % and 60 % of the ultimate load.

### 3.3. Influence of microcracks on chloride penetration

Fig. 7(a) and (b) show the longitudinal profiles (X-X profile in Fig. 2) of the specimens after 150 days immersion under sustained load level of 60 % and 75 % ultimate load, respectively. The average penetration depths in non-cracked areas of these two specimens were 6.3 mm and 6.7 mm for the load level of 60 % and 75 %, respectively. It can be noted that the penetration depths along the cracks were considerably larger than those in uncracked areas. The widths of the two measured cracks were 22.8  $\mu\text{m}$  (crack I) and 42.6  $\mu\text{m}$  (crack II) under 60 % ultimate load (Fig. 7a). In terms of 75 % ultimate load level, two main cracks with widths of 55.0  $\mu\text{m}$  (crack I) and 50.5  $\mu\text{m}$  (crack II) were observed (Fig. 7b). The penetration depths (distance from the exposed surface) were 9.9 mm (crack I) and 34.7 mm (crack II) under 60 % ultimate load, while they increased to 47.2 mm (crack I) and 44.7 mm (crack II) under 75 % ultimate load. According to the test results, the crack widths of the pure bending section and shearing-bending section of the specimen are closer at the later stage of loading.

In addition, chlorides penetrate perpendicular to the crack wall but much smaller than that occurred at the exposed surface. This is because the crack width is lower than the ‘threshold width’ generally defined around 55–80  $\mu\text{m}$ , below which the penetration appears to be a limiting factor [37,38]. It confirms that the tight crack width of ECC limits the chloride penetration along the crack path, leading to improved durability. In contrast, the tensile cracking of mortar and concrete is brittle damage with large crack width, which weakens its resistance to chloride ion erosion. Therefore, ECC has a greater performance advantage.

Fig. 7(c) shows the longitudinal section (X-X profile in Fig. 2) of the specimen pre-loaded by 60 % of the ultimate strength and 150 days of chloride solution exposure. Only one visible crack is observed. The crack has a width of 31.5  $\mu\text{m}$ , and the chloride penetration depth along the crack is 25.1 mm. The reason is that ECC has significant deflection-hardening characteristics: After unloading, the ECC specimen produces a certain degree of elastic recovery, resulting in partial recovery of cracks. Meanwhile, self-healing due to continued hydration leads to the reduction of the accessible cracks [22,39,40]. However, for specimens subjected to continuous loads, under constant bending loads, the width of the microcracks increases and the damage increases over time [41–43]. This facilitates the chloride penetration.

### 3.4. Influence of maximum normal tensile stress on chloride penetration

Influence of maximum normal tensile stress on the chloride penetration depth under sustained load condition is plotted in Fig. 8. It shows that, regardless of the exposure time, the chloride penetration depth increased with the maximum normal tensile stress. This is because the formation of transverse cracks and damage are closely related with the maximum normal tensile stress, which creates preferential pathways for chloride ingress. Similar phenomenon has been found in conventional concrete [44,45]. A linear relationship can be used to explain the correlation between the chloride penetration depth and maximum normal tensile stress at a certain exposure time. The determination coefficient ( $R^2$ ) of each fitting is above 0.9.

Fig. 9 presents the surface chloride content (in depth of 0–5 mm) of the ECC under various sustained maximum normal tensile stress and exposure time period. With the same exposure time, the surface chloride concentration gradually rose with the increased maximum normal tensile stress. With time, the influence of the normal tensile stress became more considerable. When there was no bending stress (i.e. in reference beams), the chloride concentration at 30 days, 60 days, and 150 days were 0.56 %, 0.69 %, and 0.80 %, respectively. When the maximum normal tensile stress reached 8.56 MPa, the chloride concentrations at 30 days, 60 days, and 150 days increased to 0.98 %, 1.34 %, and 1.55 %, respectively. This can be attributed to the microcracks introduced by the tensile stress as discussed above. An exponential equation can be used to describe the correlation between the surface chloride content and maximum normal tensile stress:

$$C = ae^{b\sigma_m} \quad (1)$$

where  $C$  is chloride ion content at the surface of the specimen (%),  $\sigma_m$  is the maximum normal tensile stress (MPa);  $a$  and  $b$  are fitting constants.  $a$  represents the chloride concentration with no stress, while  $b$  denotes the impact of the maximum normal tensile stress on the chloride content. High determination coefficient ( $> 0.95$ ) was found under all the immersion period, confirming the feasibility of the proposed correlation. It can be noted that  $b$  increases with the immersion time, indicating the effect of the maximum tensile stress become more considerable under the long-term exposure.

Under natural immersion environment, the main way of chloride ion penetration is diffusion. Generally, apparent chloride ion diffusion coefficient represents the diffusion rate of chloride ions in concrete materials. In practical calculations, analytical solution of Fick's second law is usually applied to calculate the apparent chloride diffusion coefficient [46].

$$C(x, t) = C_0 \left( 1 - \operatorname{erf} \frac{x}{2\sqrt{Dt}} \right) \quad (2)$$

Where  $C(x, t)$  is the chloride content (%),  $x$  (m) is diffusion depth and  $t$  (s) is exposure time,  $C_0$  is the chloride concentration of specimen surface as a boundary condition,  $D$  is the apparent chloride diffusion coefficient ( $\text{m}^2/\text{s}$ ),  $\operatorname{erf}$  is the error function.

Fig. 10 indicates the change of apparent chloride diffusion coefficient

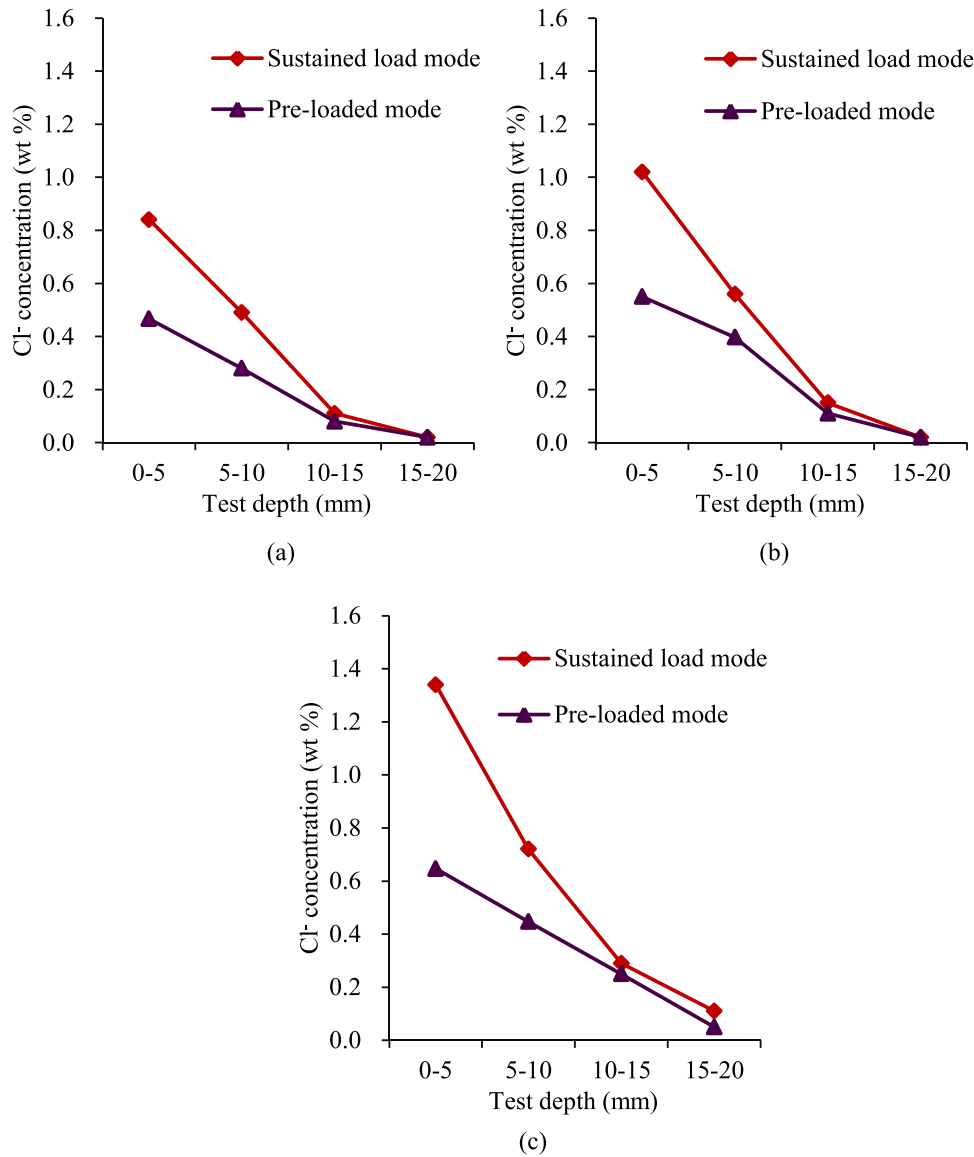


**Fig. 6.** Cl<sup>-</sup> concentration profile at C area under different loading conditions after 60 days exposure: (a): 30 % of the ultimate load; (b): 60 % of the ultimate load; (c): 75 % of the ultimate load.

with various maximum normal tensile stress and time. It was observed that the apparent chloride diffusion coefficient remained unchanged for the same bending stress, irrespective of the local shear forces. This means that the local shear force which is parallel to the chloride ion penetration direction has limited influence on the chloride transportation. Furthermore, the chloride diffusion coefficient reduced significantly as the expose time increases under the same bending stress because of the continuous hydration of cementing material as well as the formation of Friedel's salt and CaCO<sub>3</sub>, which is explained in Section 3.5. On the other hand, at the same exposure time, the apparent chloride diffusion coefficient increased as the sustained bending stress is improved. It can be noted that there exists an exponential correlation between the chloride diffusion coefficient and the maximum normal tensile stress. The following equation can correlate the apparent chloride diffusion coefficient with immersion time and maximum normal tensile stress.

$$\ln(D) = a_1 \sigma_m - b_1 \ln(t) + c_1 \quad (3)$$

Where  $D$  is apparent chloride diffusion coefficient (m<sup>2</sup>/s),  $\sigma_m$  is the maximum normal tensile stress (MPa),  $t$  is time (s);  $a_1$ ,  $b_1$  and  $c_1$  are the

fitting parameters. Regression analysis was conducted. The constant  $a_1$ ,  $b_1$  and  $c_1$  are 0.0389, 0.8386 and 4.8771 respectively with a determination coefficient ( $R^2$ ) of 0.99. The  $F$ -test was used to check whether the model provided a good fit. The test shows that the  $p$ -value of the  $F$ -statistic is 0.0001, which is much smaller than the significant level of 0.05. This confirms that the proposed model fits the data well.

### 3.5. Phase composition changes

Fig. 11 compares the XRD characteristics of specimens exposed to water and NaCl solution. It shows that, compared with the water immersion condition, the amount of Ca(OH)<sub>2</sub> (corresponding to  $2\theta$  around 18° in the XRD pattern) and SiO<sub>2</sub> was significantly reduced when the sample was exposed to NaCl solution. The main reason is that Ca(OH)<sub>2</sub> reacts with the active SiO<sub>2</sub> in fly ash to generate a C-S-H gel [6]. In addition, the amount of CaCO<sub>3</sub> and Friedel's salt increased after immersion as reflected in the XRD pattern (peak positions of  $2\theta$  were around 11.2° and 29.4° for Friedel's salt and CaCO<sub>3</sub>, respectively). This is because the hydration products of tricalcium aluminate (C<sub>3</sub>A) can react with chloride ions generating Friedel's salt. In the course, CO<sub>3</sub><sup>2-</sup> are replaced. Afterwards it further reacts with Ca(OH)<sub>2</sub> to generate CaCO<sub>3</sub>

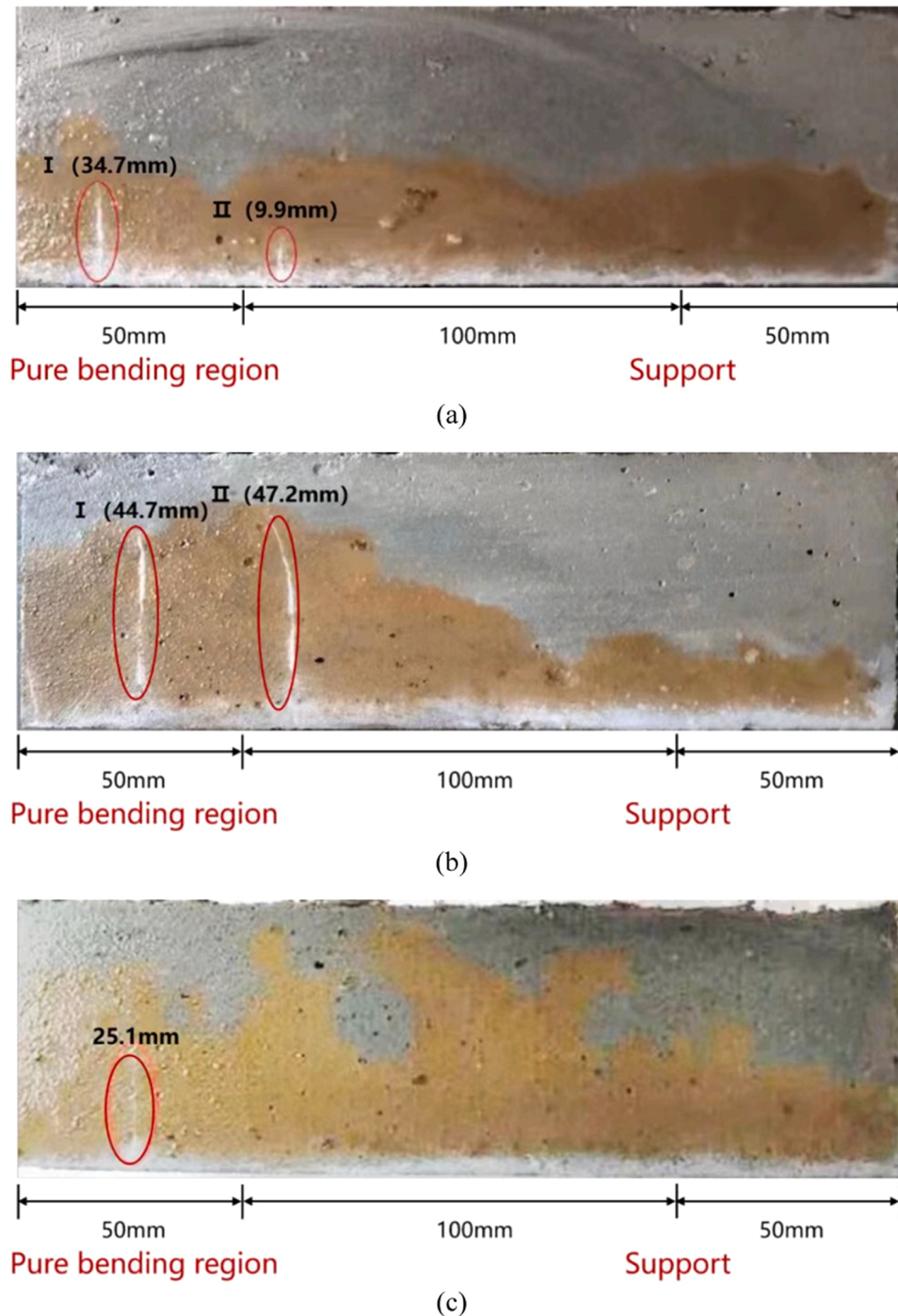


**Fig. 7.** Influence of microcracks on chloride penetration depth: (a) under 60% sustained ultimate load; (b) under sustained 75 % ultimate load; (c) under pre-loaded mode of 60 % ultimate load.

[47,48]. These products fill the pores inside the specimen and therefore reduce the porosity. Thus, the apparent chloride diffusion coefficient reduced as the immersion time increased.

Fig. 12 presents the results from the MIP measurements. It is shown that the porosity of the 28 days cured ECC was 26.22 % and it reduced to 22.31 % after 60-day exposed to the NaCl solution under sustained loading. Clearly, after immersion in NaCl, the total porosity is reduced. However, the critical pore diameter (assume the diameter corresponding to the peak in the differential pore size distribution [49]) increases. As mentioned above, the decreased total porosity can be explained by the constantly hydration of the cementitious material as well as the production of Friedel's salt and  $\text{CaCO}_3$ , while the enlarged critical pore

diameter is linked to the expansion of microcracks caused by the bending load. Compared with the total porosity, the critical pore diameter has been considered as a dominated parameter for durability of conventional concrete [50]. This also holds for the ECC as shown in the current study.

#### 4. Conclusions

In this paper, the effect of sustained flexural load on the chloride diffusion of ECC was studied. The following conclusions can be pointed out.

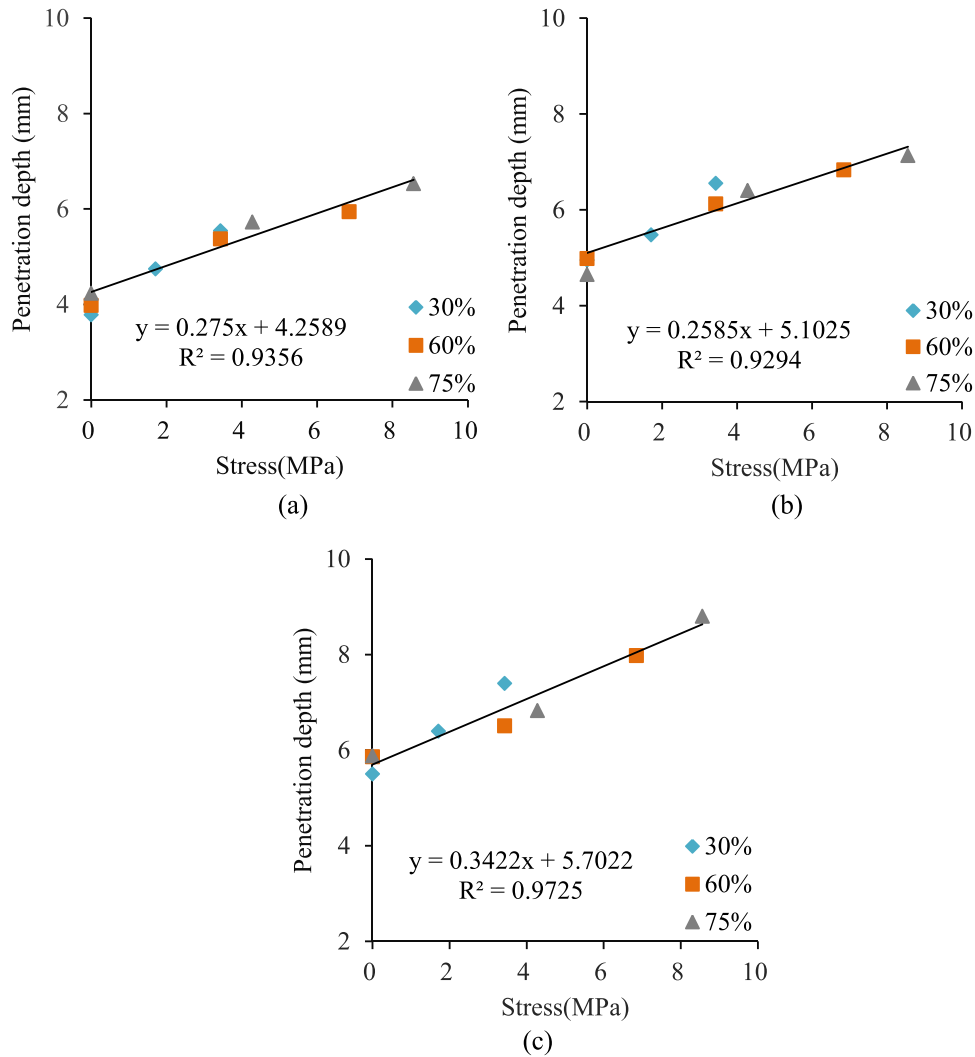


Fig. 8. Influence of sustained load on the chloride penetration depth after (a) 30 days, (b) 60 days, and (c) 150 days exposure to NaCl solution.

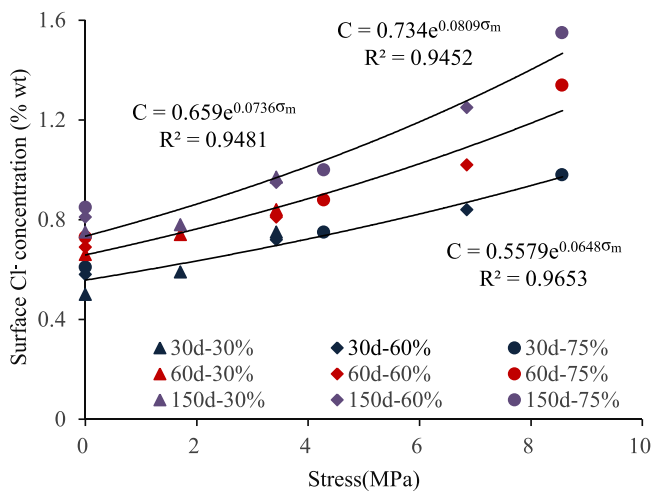


Fig. 9. Influence of sustained load on the surface chloride concentration.

- Regarding the same load level, the chloride penetration depth of specimens under sustained load is larger than that of the pre-loaded specimens. This difference increases with exposure time and load level. After 150 days exposure, the difference is larger than 20 %.

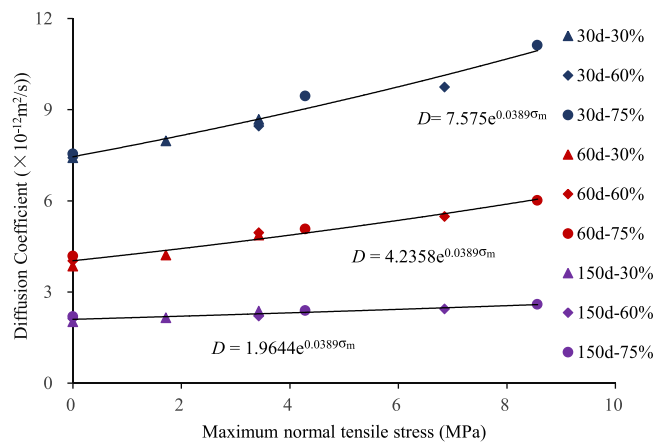


Fig. 10. Relationship between apparent chloride diffusion coefficient and maximum normal tensile stress.

- This indicates that the resistance to chloride ingress of ECC would be overestimated when using pre-loaded specimens.
- Within a certain exposure time, there is a linear correlation between chloride penetration depth and the local maximum normal tensile stress. The exponential equation can be applied to describe the

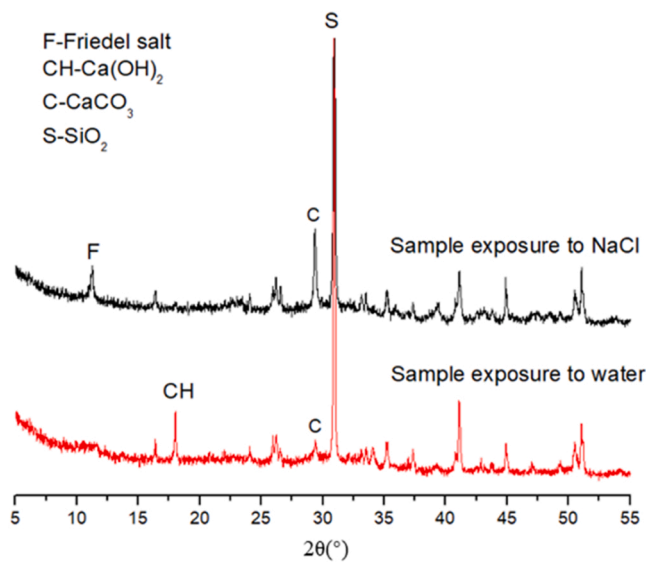


Fig. 11. XRD characteristics of two specimens immersed in water versus loaded and chloride ion solution immersed.

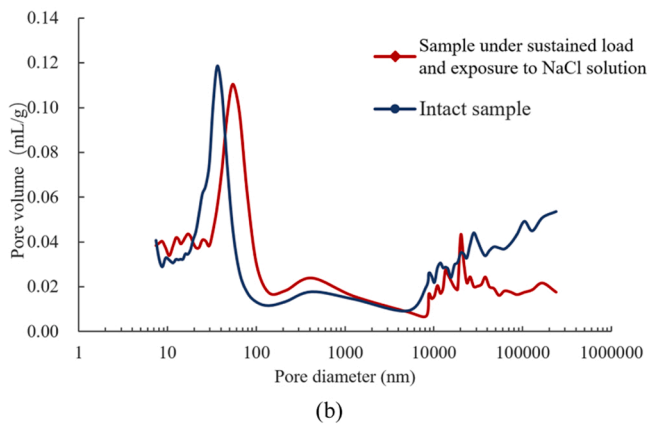
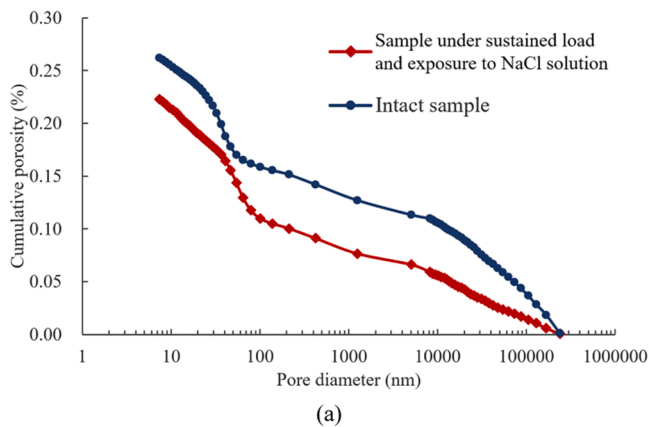


Fig. 12. The effect of coupled sustained load and NaCl solution exposure on the (a) cumulative porosity and (b) pore size distribution of ECC.

correlation between the surface chloride concentration and the sustained maximum normal tensile stress.

- Chloride ion diffusion coefficient is observed to be related to bending stresses, and it decreases with the increase of immersion time. In this regard, a binary model between chloride ion diffusion coefficient,

exposure time and bending stress is established, which has a good correlation with the test results.

- Under coupled NaCl solution exposure and continuous loading, the total porosity of ECC is reduced because of the continuous hydration of cement and FA as well as the formation of Friedel and  $\text{CaCO}_3$ . However, the critical pore diameter increases because of the sustained load, which facilitates chloride ingress. Compared with total porosity, the critical pore diameter is more dominating for the chloride transportation in ECC.

#### CRediT authorship contribution statement

**Chuan Wang:** Methodology, Supervision, Writing – review & editing. **Renjuan Sun:** Investigation, Funding acquisition. **Xinlei Hu:** Writing – original draft. **Yanhua Guan:** Methodology, Writing – review & editing. **Yingzi Yang:** Writing – review & editing. **Wei Lu:** Investigation, Methodology. **Jun Tian:** Writing – review & editing. **Hongzhi Zhang:** Methodology, Writing – review & editing, Funding acquisition. **Zhi Ge:** Methodology, Writing – review & editing. **Branko Šavija:** Methodology, Writing – review & editing.

#### Declaration of Competing Interest

The authors declare that they have no known competing financial interests or personal relationships that could have appeared to influence the work reported in this paper.

#### Data Availability

Data will be made available on request.

#### Acknowledgements

This work was supported by Natural Science Foundation of Shandong Province (ZR2021ME215), the National Natural Science Foundation of China (No. 52008234 and 51978387), Taishan Scholars Foundation of Shandong Province (No. tsqn201909032), Natural Science Foundation of Jiangsu Province (No. BK20200235) and 111 Project (B21012).

#### References

- [1] J. Zuquan, S. Wei, Z. Yunsheng, J. Jinyang, L. Jianzhong, Interaction between sulfate and chloride solution attack of concretes with and without fly ash, *Cem. Concr. Res.* 37 (8) (2007) 1223–1232.
- [2] K. Hong, R.D. Hooton, Effects of cyclic chloride exposure on penetration of concrete cover, *Cem. Concr. Res.* 29 (9) (1999) 1379–1386.
- [3] A. Ababneh, F. Benboudjema, Y. Xi, Chloride penetration in nonsaturated concrete, *J. Mater. Civ. Eng.* 15 (2) (2003) 183–191.
- [4] Q.-f. Liu, M.F. Iqbal, J. Yang, X.-y. Lu, P. Zhang, M. Rauf, Prediction of chloride diffusivity in concrete using artificial neural network: modelling and performance evaluation, *Constr. Build. Mater.* 268 (2021), 121082.
- [5] A. Raharinaivo, P. Brevet, G. Grimaldi, G. Pannier, Relationships between concrete deterioration and reinforcing-steel corrosion, *Durab. Build. Mater.* 4 (2) (1986) 97–112.
- [6] P.S. Mangat, K. Gurusamy, Chloride diffusion in steel fibre reinforced marine concrete, *Cem. Concr. Res.* 17 (3) (1987) 385–396.
- [7] A. Djerbi, S. Bonnet, A. Khelidj, V. Baroghel-bouny, Influence of traversing crack on chloride diffusion into concrete, *Cem. Concr. Res.* 38 (6) (2008) 877–883.
- [8] M. Maalej, S. Quek, S. Ahmed, J. Zhang, V. Lin, K. Leong, Review of potential structural applications of hybrid fiber engineered cementitious composites, *Constr. Build. Mater.* 36 (2012) 216–227.
- [9] H. Li, C.K. Leung, S. Xu, Q. Cao, Potential use of strain hardening ECC in permanent formwork with small scale flexural beams, *J. Wuhan Univ. Technol.-Mater. Sci. Ed.* 24 (3) (2009) 482–487.
- [10] S.B. Singh, M. Sivasubramanian, Flexural response of ECC strengthened reinforced concrete beams, *Indian Concr. J.* 87 (7) (2013) 35–44.
- [11] S. Mustafa, S. Singh, D. Hordijk, E. Schlangen, M. Luković, Experimental and numerical investigation on the role of interface for crack-width control of hybrid SHCC concrete beams, *Eng. Struct.* 251 (2022), 113378.
- [12] S.W. Victor C. Li, W. Cynthia, Tensile strain-hardening behavior of polyvinyl alcohol engineered cementitious composite (PVA-ECC), *ACI Mater. J.*, vol. 98 (no. 6).

- [13] J. Yu, J. Lin, Z. Zhang, V.C. Li, Mechanical performance of ECC with high-volume fly ash after sub-elevated temperatures, *Constr. Build. Mater.* 99 (2015) 82–89.
- [14] V.C. Li, C. Wu, S. Wang, A. Ogawa, T.J.M.J. Saito, Interface tailoring for strain-hardening polyvinyl alcohol-engineered cementitious composite (PVA-ECC), *Acta Mater.* 50 (2002) 463–472.
- [15] B. Nematollahi, J. Sanjayam, F.U.A. Shaikh, Tensile strain hardening behavior of PVA fiber-reinforced engineered geopolymer composite, *J. Mater. Civ. Eng.* 27 (10) (2015) 04015001.
- [16] C.K.Y. Leung, Y.N. Cheung, J. Zhang, Fatigue enhancement of concrete beam with ECC layer, *Cem. Concr. Res.* 37 (5) (2007) 743–750.
- [17] H.-D. Yun, K. Rokugo, T. Izuka, S.-C. Lim, Crack-damage mitigation of RC one-way slabs with a strain-hardening cement-based composite layer, *Mag. Concr. Res.* 63 (7) (2011) 493–509.
- [18] Y. Guan, J. Wu, R. Sun, H. Zhang, Y. Hu, F. Wang, Transverse flexural behaviour of steel-engineering cementitious composites (ECC) composite deck under negative and positive bending forces, *KSCE J. Civ. Eng.*, 2021.
- [19] Z. Zhang, J. Hu, H. Ma, Feasibility study of ECC with self-healing capacity applied on the long-span steel bridge deck overlay, *Int. J. Pavement Eng.* 20 (8) (2019) 884–893.
- [20] H. Ma, Z. Zhang, B. Ding, X. Tu, Investigation on the adhesive characteristics of engineered cementitious composites (ECC) to steel bridge deck, *Constr. Build. Mater.* 191 (2018) 679–691.
- [21] H. Liu, Q. Zhang, V. Li, H. Su, C. Gu, Durability study on engineered cementitious composites (ECC) under sulfate and chloride environment, *Constr. Build. Mater.* 133 (2017) 171–181.
- [22] M. Sahmaran, M. Li, V.C. Li, Transport properties of engineered cementitious composites under chloride exposure, *ACI Mater. J.* 104 (6) (2007) 604.
- [23] L. Mo, C.L. Victor, Cracking and healing of engineered cementitious composites under chloride environment, *ACI Mater. J.*, vol. 108(no. 3).
- [24] H. Liu, Q. Zhang, C. Gu, H. Su, V. Li, Self-healing of microcracks in engineered cementitious composites under sulfate and chloride environment, *Constr. Build. Mater.* 153 (2017) 948–956.
- [25] M.D. Lepech, V.C. Li, Water permeability of engineered cementitious composites, *Cem. Concr. Compos.* 31 (10) (2009) 744–753.
- [26] Y. Yang, M.D. Lepech, E.-H. Yang, V.C. Li, Autogenous healing of engineered cementitious composites under wet–dry cycles, *Cem. Concr. Res.* 39 (5) (2009) 382–390.
- [27] H. Ma, S. Qian, Z. Zhang, Effect of self-healing on water permeability and mechanical property of medium-early-strength engineered cementitious composites, *Constr. Build. Mater.* 68 (2014) 92–101.
- [28] H. Zhou, S. Chen, Y. Du, Z. Lin, X. Liang, J. Liu, F. Xing, Field test of a reinforced concrete bridge under marine environmental corrosion, *Eng. Fail. Anal.* 115 (2020), 104669.
- [29] W.S. Labiapar, R.J. Gonçalves, C.M. de Alcântara, V. Pagani, J.C. Di Cunto, J.D. B. de Mello, Understanding abrasion-corrosion to improve concrete mixer drum performance: a laboratory and field approach, *Wear* 477 (2021), 203830.
- [30] K. Kobayashi, K. Hosokawa, Y. Hattori, H.-D. Yun, Influence of bending cracks on the distribution of rebar corrosion in SHCC, *Cem. Concr. Compos.* 122 (2021).
- [31] J. Shi, J. Ming, W. Sun, Y. Zhang, Corrosion performance of reinforcing steel in concrete under simultaneous flexural load and chlorides attack, *Constr. Build. Mater.* 149 (2017) 315–326.
- [32] S.N. Nobuaki Otsuki, N. Kenji, Evaluation of AgNO<sub>3</sub> solution spray method for measurement of chloride penetration into hardened cementitious matrix materials, *ACI Mater. J.*, vol. 89(no. 6).
- [33] Q. Yuan, C. Shi, F. He, G. De Schutter, K. Audenaert, K. Zheng, Effect of hydroxyl ions on chloride penetration depth measurement using the colorimetric method, *Cem. Concr. Res.* 38 (10) (2008) 1177–1180.
- [34] M.-Y. Kim, E.-I. Yang, S.-T. Yi, Application of the colorimetric method to chloride diffusion evaluation in concrete structures, *Constr. Build. Mater.* 41 (2013) 239–245.
- [35] B. Slomka-Stupik, J. Podworny, M. Staszuk, Corrosion of cement pastes made of CEM I and CEM III/A caused by a saturated water solution of ammonium chloride after 4 and 25 days of aggressive immersion, *Constr. Build. Mater.* 170 (2018) 279–289.
- [36] R. Sun, X. Hu, Y. Ling, Z. Zuo, P. Zhuang, F. Wang, Chloride diffusion behavior of engineered cementitious composite under dry-wet cycles, *Constr. Build. Mater.* 260 (2020), 119943.
- [37] M. Ismail, A. Touni, R. François, R. Gagné, Effect of crack opening on the local diffusion of chloride in cracked mortar samples, *Cem. Concr. Res.* 38 (8–9) (2008) 1106–1111.
- [38] S.Y. Jang, B.S. Kim, B.H. Oh, Effect of crack width on chloride diffusion coefficients of concrete by steady-state migration tests, *Cem. Concr. Res.* 41 (1) (2011) 9–19.
- [39] M. Li, V.C. Li, Cracking and healing of engineered cementitious composites under chloride environment, *ACI Mater. J.* 108 (3) (2011).
- [40] S. Qian, J. Zhou, M.R. de Rooij, E. Schlangen, G. Ye, K. van Breugel, Self-healing behavior of strain hardening cementitious composites incorporating local waste materials, *Cem. Concr. Compos.* 31 (9) (2009) 613–621.
- [41] L. Higgins, J.P. Forth, A. Neville, R. Jones, T. Hodgson, Behaviour of cracked reinforced concrete beams under repeated and sustained load types, *Eng. Struct.* 56 (2013) 457–465.
- [42] L. Hariche, Y. Ballim, M. Bouhicha, S. Kenai, Effects of reinforcement configuration and sustained load on the behaviour of reinforced concrete beams affected by reinforcing steel corrosion, *Cem. Concr. Compos.* 34 (10) (2012) 1202–1209.
- [43] J. Wu, P.N. Faye, W. Zhang, B.J.C. Diao, B. Materials, Chloride diffusivity and service life prediction of RC columns with sustained load under chloride environment, *Constr. Build. Mater.* 158 (2018) 97–107.
- [44] H. Wang, C. Lu, W. Jin, Y. Bai, Effect of external loads on chloride transport in concrete, *J. Mater. Civ. Eng.* 23 (7) (2011) 1043–1049.
- [45] C. Fu, H. Ye, N. Jin, Y. Huang, Chloride penetration in reinforced concrete beams under combined sustained loading and drying–wetting cycles, *J. Mater. Civ. Eng.* 32 (4) (2020).
- [46] E. Poulsen, L. Mejlbro, *Diffusion of Chloride in Concrete: Theory and Application*, CRC Press, 2010.
- [47] M.V.A. Florea, H.J.H. Brouwers, Chloride binding related to hydration products: Part I: Ordinary Portland cement, *Cem. Concr. Res.* 42 (2) (2012) 282–290.
- [48] F. Shaheen, B. Pradhan, Influence of sulfate ion and associated cation type on steel reinforcement corrosion in concrete powder aqueous solution in the presence of chloride ions, *Cem. Concr. Res.* 91 (2017) 73–86.
- [49] K. Scrivener, R. Snellings, B. Lothenbach, *A Practical Guide to Microstructural Analysis of Cementitious Materials*, Crc Press, 2018.
- [50] P. Halamickova, R.J. Detwiler, D.P. Bentz, E.J. Garboczi, Water permeability and chloride ion diffusion in portland cement mortars: relationship to sand content and critical pore diameter, *Cem. Concr. Res.* 25 (4) (1995) 790–802.